ALMA MATER STUDIORUM
UNIVERSITÀ DI BOLOGNA

ARCHIVIO ISTITUZIONALE
DELLA RICERCA

Alma Mater Studiorum Università di Bologna
Archivio istituzionale della ricerca

Conical Intersections Studied by the Configuration-Interaction-Corrected Tamm-Dancoff Method

This is the final peer-reviewed author's accepted manuscript (postprint) of the following publication:

Published Version:
Xu, L., Freixas, V.M., Aleotti, F., Truhlar, D.G., Tretiak, S., Garavelli, M., et al. (2025). Conical Intersections Studied by the Configuration-Interaction-Corrected Tamm-Dancoff Method. JOURNAL OF CHEMICAL THEORY AND COMPUTATION, 21(7), 3600-3611 [10.1021/acs.jctc.4c01768].

Availability:
This version is available at: https://hdl.handle.net/11585/1031155 since: 2025-12-03

Published:
DOI: http://doi.org/10.1021/acs.jctc.4c01768

Terms of use:

Some rights reserved. The terms and conditions for the reuse of this version of the manuscript are specified in the publishing policy. For all terms of use and more information see the publisher's website.

This item was downloaded from IRIS Università di Bologna (https://cris.unibo.it/).
When citing, please refer to the published version.

(Article begins on next page)

09 November 2026

Conical Intersections Studied by the Configuration-Interaction-Corrected Tamm-Dancoff Method

Lei Xu,[*,†] Victor M. Freixas,[‡] Flavia Aleotti,[¶] Donald G. Truhlar,[§] Sergei Tretiak,[‖,⊥] Marco Garavelli,[¶] Shaul Mukamel,[‡] and Niranjan Govind[*,†,#]

†*Physical and Computational Sciences Directorate, Pacific Northwest National Laboratory, Richland, WA 99352, USA*

‡*Department of Chemistry and Department of Physics and Astronomy, University of California, Irvine, California 92697-2025, USA*

¶*Dipartimento di Chimica Industriale "Toso Montanari", University of Bologna, Via Piero Gobetti 85, Bologna 40129, Italy*

§*Department of Chemistry, Chemical Theory Center, and Minnesota Supercomputing Institute, University of Minnesota, Minneapolis, MN 55455-0431, USA*

‖*Physics and Chemistry of Materials, Theoretical Division, Los Alamos National Laboratory, Los Alamos, New Mexico 87545, USA*

⊥*Center for Integrated Nanotechnologies, Los Alamos National Laboratory, Los Alamos, New Mexico 87545, USA*

#*Department of Chemistry, University of Washington, Seattle, WA 98195, USA*

E-mail: lei.xu@pnnl.gov; niri.govind@pnnl.gov

Abstract

Conical intersections directly mediate the internal energy conversion in photoin-

duced processes in a wide range of chemical and biological systems. Because of the Brillouin theorem, many conventional electronic structure methods, including configuration interaction with single excitations from a Hartree-Fock reference and time-dependent density functional theory in either the linear response approximation (TDDFT) or Tamm-Dancoff approximation (DFT-TDA), have the wrong dimensionality for conical intersections between the ground state (S_0) and the first excited state (S_1) of the same multiplicity. This leads to unphysical state crossings. Here, we implement and assess the configuration-interaction-corrected Tamm-Dancoff approximation (CIC-TDA) that restores the correct dimensionality of conical intersections by including the coupling between the reference state and the intersecting excited state. We apply the CIC-TDA method to the S_1/S_0 conical intersections in ammonia (NH_3), ethylene (C_2H_4), bithiophene ($C_8H_6S_2$), azobenzene ($C_{12}H_{10}N_2$), and 11-cis retinal protonated Schiff base (PSB11) in vacuo. We show that this black-box approach can produce potential energy surfaces (PESs) of comparable accuracy to multireference wave function methods. The method validated here can allow cost-efficient explorations of photoinduced electronically nonadiabatic dynamics, especially for large molecules and complex systems.

Introduction

Conical intersections (CoIns)[1–10] play a central role in many crucial photochemical and photobiological processes, such as photosynthesis and light-harvesting,[11] photocatalysis,[12] photoisomerization in the primary event of vision,[13,14] and ultraviolet light-induced DNA damage.[15–17] CoIns are a common feature of molecular potential energy surfaces (PESs) when two or more electronic states become degenerate. At and near the CoIn seams, the Born-Oppenheimer approximation breaks down, resulting in strongly coupled electronic and nuclear degrees of freedom. The dynamics of polyatomic molecules in excited states are often driven by internal energy conversion at CoIns and frequently leads to photodissociation or

photoisomerization processes. The strong coupling at the intersections may bifurcate the nuclear wave packet such that each portion evolves along a different PES, and the ultrafast nonradiative decay in the vicinity of a CoIn often controls the proportions of the various photoproducts. Therefore, the development of efficient computational techniques for the proper description of CoIns is crucial for studying photochemical processes in molecular systems.

Multireference (MR) electronic structure methods are important for treating the correlation of degenerate and nearly degenerate states, and they are often used to compute consistent PESs of the ground and excited states.[18,19] Such methods include multistate complete active space perturbation theory (MS-CASPT2),[20] based on complete active space self-consistent field (CASSCF) reference functions, and multireference configuration interaction (MRCI).[21–23] However, MR methods require a careful selection of orbitals in the active space, and their intrinsic complexity often requires system-specific specialized knowledge for their effective application. In addition, MR computations are often very expensive, making them less than ideal for running nonadiabatic dynamics on moderate-sized and large molecules especially when the dynamics calculations require extensive ensemble averaging and/or long time scales.

Considering the favorable combination of computational cost and semi-quantitative accuracy of Kohn-Sham density functional theory (KS-DFT),[24,25] time-dependent density functional theory (TDDFT)[26,27] is a popular method for treating electronically excited states of molecules, where calculations may be performed in the linear-response approximation (KS-LR) or the Tamm-Dancoff approximation (KS-TDA). In the rest of this article, we will follow the usual convention of labeling KS-LR simply as TDDFT. Unlike MR methods, TDDFT and KS-TDA are based on singly excited Slater determinants. The working equation of TDA closely resembles that of conventional configuration interaction with single excitations from a Hartree-Fock reference (HF-CIS).[28] In this framework, doubly excited configurations are missing in the response state, so the coupling between the ground state and singly excited

states is always zero according to the Brillouin theorem.[29–31] We note that if doubly excited states are included in the configuration interaction, the ground and singly excited states could mix indirectly through the doubly excited states. The identically zero coupling of the approximate ground singlet state (S_0) and the first singly excited singlet state (S_1), gives the wrong dimensionality to the CoIn seam between them.[18] In particular, if a molecule has F internal nuclear degrees of freedom, the CoIn seam should have a dimension of $F-2$, but HF-CIS, TDDFT, and KS-TDA all predict a seam of dimension $F-1$. Likewise, conventional algebraic-diagrammatic construction (ADC) methods, which usually rely on the HF ground state as the starting point, are unable to reproduce the correct dimensionality and conical shape of an S_1/S_0 surface crossing.[32,33] For coupled-cluster theory, such as the equation-of-motion coupled-cluster (EOM-CC) and multireference coupled-cluster (MR-CC), problems in the vicinity of accidental same-symmetry intersections can be anticipated due to the inherent non-Hermitian character of the ansatz.[34–36]

Various modifications of TDDFT have been proposed to improve the description of excited states in the context of CoIns. Grimme and Waletzke[37] presented a semi-empirical approach in which the configuration interaction matrix elements are constructed empirically by using the exact operator and corrections from DFT. Gräfenstein and Cremer[38] proposed the CAS-DFT method which allows an economical, simultaneous treatment of static and dynamic correlation effects for systems with MR character. Spin-flip TDDFT[39,40] methods that describe target multiconfigurational states as spin-flipping excitations from a single-configurational high-spin triplet reference have shown good performance for CoIns in ethylene-like and uracil molecules.[41–43] More recently, mixed-reference spin-flip TDDFT extensions have been introduced by Park *et al.*[44] to tackle this problem.

Another approach is multiconfiguration pair-density functional theory (MC-PDFT)[45,46] in which a multiconfiguration reference wave function is combined with DFT to provide a better treatment of strongly correlated systems. However, MC-PDFT is a single-state method in which the final MC-PDFT energies do not come from the diagonalization of a

model-space Hamiltonian matrix, thus this can lead to the wrong topology at CoIns.[47,48] Multistate extensions of MC-PDFT have been developed, such as compressed multistate PDFT[47,48] (CMS-PDFT) and linearized PDFT[49] (L-PDFT), in order to recover the correct topology of CoIn. But for the structures of nearly linear molecules, the CMS-PDFT energies are nonunique and can be discontinuous.[49] L-PDFT does not fail for the degenerate states of nearly linear molecules and its computational cost scales as a constant with the number of states included in the state averaging.[49] It was recently demonstrated that L-PDFT can be used for the study of azomethane nonadiabatic molecular dynamics.[50]

Maitra and co-workers[51,52] have explored the dressed TDDFT (D-TDDFT) model which explicitly included two hole−two particle states (*i.e.*, double excitations) by adding frequency-dependent terms from many−body theory to the adiabatic exchange-correlation kernel. Huix-Rottlant introduced an approach called Brillouin-corrected dressed TDDFT (b-D-TDDFT) as an extension to D-TDDFT.[53] A parameterized treatment combining HF-CIS or a parameterized semi-empirical TDDFT with one doubly excited configuration has also been proposed to recover the correct dimensionality of CoIns.[54,55]

Most of the above enhancements involve an increase in computational effort and complexity that may limit their applicability to nonadiabatic dynamics simulations. An additional drawback of semi-empirical TDDFT approaches is the quality and transferability of the parameters upon which these theories are based. This issue is even more critical for nonadiabatic dynamics simulations, which explore regions far away from those employed for parametrization.

Simple alternatives to the above approaches are configuration-interaction-corrected TDA (CIC-TDA)[56] and dual-functional TDA (DF-TDA)[57] in which another set of orbitals is used instead of KS self-consistent orbitals when building the KS-TDA Hamiltonian. The CIC-TDA method offers a well-defined and cost-effective way to remedy the incorrect dimensionality of CoIns within KS-TDA. Here we investigate the CIC-TDA method to treat PESs corresponding to bond making and bond breaking processes of large molecules mediated by

CoIns and compare our results to those obtained by wave function calculations.

Theory

Within TDDFT, the excitation energies are obtained by solving the following non-Hermitian eigenvalue equation:[26,27,58,59]

$$\begin{pmatrix} \mathbf{A} & \mathbf{B} \\ \mathbf{B}^* & \mathbf{A}^* \end{pmatrix} \begin{pmatrix} \mathbf{X} \\ \mathbf{Y} \end{pmatrix} = \omega \begin{pmatrix} 1 & 0 \\ 0 & -1 \end{pmatrix} \begin{pmatrix} \mathbf{X} \\ \mathbf{Y} \end{pmatrix} \tag{1}$$

Here, $\mathbf{A}$ and $\mathbf{B}$ denote matrices that can be represented in a basis of occupied and unoccupied eigenstates of the ground-state Kohn-Sham equations, ω is the excitation energy, and the eigenvectors $\mathbf{X}$ and $\mathbf{Y}$ represent the transition amplitudes associated with the excitations. When using a global-hybrid exchange-correlation (xc) functional with a fraction c_{HF} of Hartree-Fock exchange (where $0 < c_{\mathrm{HF}} < 1$), the matrix elements A and B are given as:[60,61]

$$\begin{aligned} A_{ia,jb} = \delta_{ij}\delta_{ab}(\epsilon_a - \epsilon_i) + (ia|bj) - c_{\mathrm{HF}}(ij|ab) \\ + (1 - c_{\mathrm{HF}})(ia|f_{\mathrm{xc}}|bj) \end{aligned} \tag{2}$$

$$B_{ia,jb} = (ia|jb) - c_{\mathrm{HF}}(ib|aj) + (1 - c_{\mathrm{HF}})(ia|f_{\mathrm{xc}}|jb) \tag{3}$$

where $(ij|ab)$ is a two-electron integral, i and j indices denote occupied orbitals, a and b denote unoccupied orbitals, ϵ_a is an orbital energy, and f_{xc} is the exchange-correlation kernel given as the second derivative of the ground-state functional. Neglecting the contributions from the $\mathbf{B}$ block and diagonalizing only $\mathbf{A}$, yields the Tamm-Dancoff approximation (TDA):[61]

$$\mathbf{AX} = \omega\mathbf{X} \tag{4}$$

The TDA includes only single excitations from occupied to virtual orbital, whereas the full linear response of Eq.(1) also allows virtual to occupied de-excitations. The TDA is a well established and widely used simplification to the full time-dependent DFT response problem. For studying photochemical dynamics, KS-TDA is often preferred to TDDFT because it is more resilient and yields no significant failure near state interactions.[62–64]

In wave function theory, the TDA corresponds to configuration interaction (CI) in which only single excitations from a Hartree-Fock determinant are included (HF-CIS). The matrix corresponding to $\mathbf{A}$ in HF-CIS theory (built from HF orbitals) is:

$$\begin{aligned} H_{ia,jb} &= \langle \Phi_i^a | H | \Phi_j^b \rangle \\ &= \delta_{ij}\delta_{ab}(\epsilon_a - \epsilon_i) + (ai|jb) - (ab|ji) \end{aligned} \tag{5}$$

where Φ_i^a denotes the singly excited determinant with an electron excited from occupied orbital i to virtual orbital a. The matrices $\mathbf{A}$ of Eq.4 and H of Eq.5 involves all single determinants except the ground-state determinant Φ_0^{HF}, which is not needed because the coupling between the ground-state determinant and any single excited determinant vanishes by virtue of Brillouin's theorem:

$$H_{0,ia} = \langle \Phi_0^{\mathrm{HF}} | H | \Phi_i^a \rangle = (a|f^{\mathrm{HF}}|i) \equiv 0 \tag{6}$$

where f^{HF} is the Fock operator as defined as:

$$f^{\mathrm{HF}} = h + \sum_i^{N^{\mathrm{occ}}} 2J_i - \sum_i^{N^{\mathrm{occ}}} K_i \tag{7}$$

where h is the core operator (kinetic energy plus external potential), J_i is the Coulomb operator, K_i is the exchange operator, and the sum is over all doubly occupied HF orbitals. The argument has just been given for HF-CIS, but the same situation holds for KS-TDA because the KS reference ground state Φ_0^{HF} does not couple to singly excited determinants.

The lack of coupling of Φ_0^{HF} to singly excited determinants in HF-CIS does not mean that there are no singly excited determinants in the exact ground state. The $|\Phi_i^a\rangle$ and $|\Phi_0\rangle$ can couple indirectly through the doubly excited determinants by including the matrix elements $\langle\Phi_0^{\mathrm{HF}}|H|\Phi_i^a\rangle$ and $\langle\Phi_0^{\mathrm{HF}}|H|\Phi_{ij}^{ab}\rangle$ in the configuration interaction Hamiltonian.[29,31] The artificial decoupling between ground state and singly excited state is the cause of the incorrect $(F-1)$ dimensionality of CoIns between the ground state and the excited state in HF-CIS and KS-TDA.

In order to correct the dimensionality of CoIns obtained from KS-TDA for the calculation of excited states, we adopt the configuration interaction-corrected TDA (CIC-TDA) method proposed earlier.[56] The CIC-TDA method introduces a non-zero coupling between the DFT ground state and single-excitation TDDFT response states by expanding $\mathbf{A}$ to a new matrix $\mathbf{A}'$ defined by:

$$\mathbf{A}' = \begin{pmatrix} E^{\mathrm{KS}} & \mathbf{c}^{\mathbf{T}} \\ \mathbf{c} & \mathbf{A} \end{pmatrix} \tag{8}$$

where E^{KS} is the energy of reference ground-state, $\mathbf{c}$ is a $(N^{\mathrm{occ}}{\cdot}N^{\mathrm{virt}})$-dimensional column vector and $\mathbf{c}^{\mathbf{T}}$ corresponds to the transpose of $\mathbf{c}$:

$$\mathbf{c}^{\mathbf{T}} = \begin{pmatrix} 0 & \cdots & 0 & A_{0,ia}^{\mathrm{CIC}} & 0 & \cdots & 0 \end{pmatrix} \tag{9}$$

The $\mathbf{c}$ vector has only one non-zero element, $A_{0,ia}^{\mathrm{CIC}}$, which is in the row of the dominant determinant of the intersecting excited state of the CoIn. The element $A_{0,ia}^{\mathrm{CIC}}$ adds the coupling between the closed-shell determinant of the ground state and the intersecting dominant singly excited determinant. It can be explicitly calculated according to wave function theory by assuming that the KS and the TDA determinants both approximate wave functions of the

real system:

$$
\begin{aligned}
A^{\mathrm{CIC}}_{0,ia} &= \langle \Phi^{\mathrm{KS}}_0 | H | \Phi^a_i \rangle = (a|h + \sum_n^{N^{\mathrm{occ}}} 2J_n - \sum_n^{N^{\mathrm{occ}}} K_n|i) \\
&= (a|h + \sum_n^{N^{\mathrm{occ}}} 2J_n + \upsilon_{\mathrm{xc}}|i) - (a|\sum_n^{N^{\mathrm{occ}}} K_n|i) - (a|\upsilon_{\mathrm{xc}}|i) \\
&= (a|f^{\mathrm{KS}}|i) - (a|\sum_n^{N^{\mathrm{occ}}} K_n|i) - (a|\upsilon_{\mathrm{xc}}|i) \\
&= -(a|\sum_n^{N^{\mathrm{occ}}} K_n|i) - (a|\upsilon_{\mathrm{xc}}|i)
\end{aligned} \tag{10}
$$

where f^{KS} is the KS operator and υ_{xc} is the exchange-correlation potential defined as the functional derivative of the xc functional E_{xc} with respect to electron density. Since the KS orbitals are not eigenvectors of the Fock operator, $A^{\mathrm{CIC}}_{0,ia}$ in eq (10) does not vanish, and its magnitude is usually small as discussed in Ref. 56 and equal to the difference between the matrix elements of HF exchange potential and KS xc potential.[56] This introduces a mixing between the singly excited $|\Phi^a_i\rangle$ and ground state $|\Phi^{\mathrm{KS}}_0\rangle$ determinants and works around the Brillouin's theorem. Introducing the coupling term $A^{\mathrm{CIC}}_{0,ia}$ between the KS ground state and its first single excitations is essential to recover the correct dimensionality and thus the double cone topology of the PESs near the S_1/S_0 CoIn.[56,57] Note that we construct the coupling term $A^{\mathrm{CIC}}_{0,ia}$ using the HF exchange functional in this work; in fact one can use any approximate xc functional to build $A^{\mathrm{CIC}}_{0,ia}$ as long as it is different from the one used in the KS self-consistent consistent solution.

The eigenvalues of CIC-TDA Hamiltonian eq (8) are found by using the Davidson iterative algorithm,[65] which is significantly less expensive than a direct diagonalization.

Computational Details

We compare and discuss results obtained with KS-SCF/KS-TDA, CIC-TDA, MRCI, and CASPT2. Calculations were performed on test cases with increasing molecular sizes. All

calculations were performed with 6-31+G(d)[66–68] basis set. In the discussion of the results, we note that: (1) in KS-SCF/KS-TDA, the S_0, S_1, and S_2 states correspond to the KS ground singlet state (KS-SCF) and the first and second excited singlet state (KS-TDA), respectively; (2) in CIC-TDA, the S_0, S_1, and S_2 states correspond to the three lowest eigenvalues of singlet states obtained by diagonalizing CIC-TDA Hamiltonian.

We implemented the CIC-TDA method in a development version of the NWChem[69,70] computational chemistry program. We used the PBE0 exchange-correlation functional,[71] which has c_{HF} equal to 0.25. We also used a variation of PBE0 where c_{HF} is equal to 0.33,[72,73] which will be referred to as PBE33. In the test cases considered here, the first excited electronic state S_1 is dominated by a transition from the highest occupied molecular orbital (HOMO) to the lowest unoccupied molecular orbital (LUMO). Thus, the corresponding single coupling matrix element and its transpose are calculated and added to the KS-TDA **A** matrix.

The MRCI calculations were carried out with the MOLPRO quantum chemistry package.[74] The CASPT2 calculations on the PSB11 system were carried out with the OpenMolcas[75] package with the same active space, *i.e.*, 12 $\pi-$electrons in 12 $\pi-$orbitals, as reported in Ref. 76, with state averaging over the two lowest-energy singlet states (S_0 and S_1) and using an imaginary shift of 0.2 E_{h} and the IPEA shift set to zero.

Results and Discussion

Ammonia

The PESs and CoIns of ammonia (NH_3) have been very well discussed in previous studies.[54–57,77–79] For NH_3, we investigate the PESs around two geometries. One is the minimum-energy CoIn (MECI) planar geometry with C_1 symmetry optimized by CASPT2 in Ref. 57. The corresponding PESs in Fig.1(c) were calculated along N-H bond distance stretch, as indicated in Fig.1(a). The other is the geometry used previously[56,79] as indicated in Fig.1(b):

r_1, r_2, and r_3 are the N−H bond lengths, θ (θ_1, θ_2, and θ_3) are the H−N−H bond angles, β is the angle between the vector trisecting the three N−H bonds and any of the N−H bonds. The PESs in Fig.1(d) was calculated along the N−H bond stretching r_1 with r_2=r_3=1.04 Å, θ= 120°, and β= 89°. For the MRCI calculations of NH_3, we used an active space of eight electrons in seven orbitals in the CASSCF calculations and the state-averaged self-consistent field (SCF) optimization was carried out for an average of three singlet states associated with this manifold; on top of the CASSCF reference, the MRCI expansion additionally includes single and double excitations.

In Fig.1(c) the KS-SCF/KS-TDA PES shows two spurious crossings between S_0/S_1 around N−H distance 2.1 Å and 2.3 Å. In contrast, CIC-TDA provides the correct crossing of CoIn around 2.1 Å and compares well with the CoIn around 1.95 Å predicted from MRCI results. Similarly, in Fig.1(d), the KS-SCF/KS-TDA PES gives an unphysical S_0/S_1 crossing at N−H bond stretching r_1=2.21 Å. This unphysical crossing is corrected by the CIC-TDA, opening a small energy gap around 0.06 eV between S_0 and S_1, which is consistent with the gap of 0.13 eV between S_0 and S_1 around r_1=2.00 Å obtained from MRCI results.

It should be noted that as shown in Fig.1(c) and Fig.1(d), the PESs of S_0 obtained from MRCI results increase initially then decrease as the N−H bond is stretched, eventually reaching a plateau at large internuclear distances [r(N−H) $\sim$ 2.5 Å in Fig. 1(c) and r(N−H) $\sim$ 2.3 Å in Fig.1(d)]. However, for example, in Fig.1(c) the PESs of S_0 calculated from KS-TDA increase continuously then reaching a plateau at N−H dissociation, and the corresponding dissociation energy [the energy difference of S_0 between r(N−H) = 1.0 Å and 3.0 Å] is 7.15 eV for KS-TDA; the CIC-TDA brings slight decrease of such dissociation energy by 0.008 eV. The example indicates that CIC-TDA corrects the S_0/S_1 crossing of KS-TDA without changing the dissociation energy since the determinant of doubly excitation from LUMO relevant for describing bond dissociation is not included in CIC-TDA Hamiltonian.

Ethylene

The PESs and CoIns of ethylene have also been extensively studied.[54–57,80–83] For C_2H_4, we use the geometry optimized with CASPT2 as in Ref. 57. The PESs computed by KS-SCF/KS-TDA, CIC-TDA, and MRCI methods along the pyramidalization angle as indicated in Fig.2(a), are shown in Fig.2(b). The reference for the MRCI calculations used an active space of two electrons in two orbitals (HOMO and LUMO) and averaging of three singlet states; all electrons were correlated. We notice that the KS ground-state solutions are relatively unstable near state crossings and in regions where the KS closed-shell reference is not the ground state, thus it is difficult to converge to smooth potential energy curves for KS-SCF/KS-TDA and CIC-TDA, as also pointed out in an earlier study.[56] The PESs calculated from KS-SCF/KS-TDA and CIC-TDA using the PBE0 functional show jumps (see Fig.S1 in Supporting Information). The smooth PESs shown in Fig.2(b) were obtained using the PBE33 functional ($c_{\mathrm{HF}} = 0.33$). The artificial crossing between S_0 and S_1 obtained from KS-SCF/KS-TDA around pyramidalization angle 2° is corrected by the CIC-TDA method. The CIC-TDA method gives a tiny energy gap around 0.13 eV between S_0 and S_1 at 2°, which agrees well with 0.08 eV at around 0° as predicted by MRCI calculations.

Bithiophene

The photophysical properties of thiophene-based materials are used in a variety of different applications,[85] such as light emitting devices[86] and polymer-based organic solar cells.[87] The radiationless-decay of the thiophene molecule after excitation is mainly associated with internal conversion via its singlet electronic states through a CoIn.[84] For bithiophene, the photo-deactivation path is dominated by an intersystem crossing (ISC) according to the study in Ref. 84. The optimized ground state geometry with the B3LYP functional with 6-311G** basis set, as shown in Fig.3(a), was reported in Ref. 84. Along the reaction path, two S_1 minimum-energy structures were optimized with CASSCF calculations with the $6-31G^{\star}$ basis sets: the S_1-min-a and S_1-min-b, corresponding to closed-ring and open-ring structures

as shown in Fig.3(b) and in Fig.3(c), respectively.

The PESs for the S_0, S_1, and S_2 states along the linear interpolation coordinate starting from the S_0 equilibrium structure to the S_1-min-a structure and continuing to the open ring S_1-min-b structure, are calculated by KS-SCF/KS-TDA and CIC-TDA methods. The corresponding results are shown in Fig.3(d) and Fig.3(e). Both KS-SCF/KS-TDA and CIC-TDA yield an S_1/S_0 crossing at interpolation coordinate ξ=1.9. However, for the crossing with KS-SCF/KS-TDA, the energy of S_1 state drops below that of S_0 state, corresponding to negative excitation energy, which is spurious and unphysical. With CIC-TDA method, the unphysical crossing is corrected at the same interpolation coordinate ξ without changing the overall profile of PESs. The CoIn obtained from CIC-TDA shown in Fig.3(e) is in good agreement with the published results using the equation of motion-coupled cluster singles and doubles method (EOM-CCSD)[84] and the TDDFT-1D[55] method.

Azobenzene

The most interesting feature of the azobenzene and its derivatives is their ability to undergo fast, efficient, and fully reversible photo-isomerization. Absorption of photons leads to internal rotation of the phenyl rings about the azo bond, converting the molecule from the *trans* to the *cis* conformation. The photoconversion between the *trans* and *cis* isomers is related to the torsion around the N=N bond and in-plane inversion of one of the two CNN angles. Previous work[88] has analyzed the PESs of S_0 and S_1 of azobenzene in the three-dimensional space spanned by CNNC torsion and the two CNN bending angles at single-state and multi-state RASPT2 levels of theory. The optimized ground-state geometries of *trans*- and *cis*-azobenzene isolated isomers in gas phase reported in Ref. 88 (as indicated in Fig.4), obtained with Møller Plesset perturbation theory (MP2), were chosen as the starting coordinates for the rigid scan of selected torsional and bending angles.

We chose the CNNC torsion angle at 180°, 100°, and 0°, and for these selected values of CNNC dihedral, we scanned the two CNN/NNC bending angles from 100° to 160° with steps

of 2°. We additionally chose the CNN bending angle at 156° with CNNC angle changing from 0° to 180° with steps of 10°. The corresponding PESs obtained from KS-SCF/KS-TDA, CIC-TDA, and RASPT2 calculations are shown in Fig.5(a-h). The RASPT2 points of S_0 and S_1 connected by dashed lines were digitized from Ref. 88. The curves for a CNNC angle of 0° in Fig.5(e) and Fig.5(f) have discontinuous derivatives due to the merging of the *trans* and *cis* rigid scans.[88] The KS-SCF/KS-TDA results give unphysical S_1/S_0 crossings as demonstrated in Fig.5(a,c,e,g). The CIC-TDA results, however, correct this and provide topologically correct CoIns without changing the overall profile of the PESs, as shown in Fig.5(b,d,f,h).

Furthermore, we compared the positions of CoIns to the RASPT2 results. For the PESs with the CNNC angle equal to 180° in Fig.5(a)-5(b), the CIC-TDA method gives the avoided crossing at CNN angle of 152°, in good agreement with the crossing at a CNN angle of 150° in the RASPT2 results. At a CNNC angle of 100°, the avoided crossing of CIC-TDA is around a CNN angle of 134°, in line with 144° in the RASPT2 results. We notice that there is a discontinuity starting from a CNN angle of 154° in the KS-SCF S_0 PES. The CIC-TDA results, in contrast, have smooth PESs with a very narrow S_1/S_0 gap around 0.2 eV after the CNN CoIn angle $>$ 134°. Similarly, the RASPT2 results show an S_1/S_0 gap of the same magnitude around 0.1 eV after a CNN CoIn angle $>$ 144°. Both CIC-TDA and RASPT2 results give PESs with steep gradient at a CNNC angle of 0° as shown in Fig.5(f). The S_1/S_0 CoIn of the CIC-TDA results is around a CNN angle of 159°, which is similar to 156° in RASPT2 results. The PESs of S_1 and S_0 at a CNN angle of 156° are rather flat in Fig.5(h). The RASPT2 results indicate a wide crossing seam covering CNNC angles from 0° to 30° and a possible CoIn around a CNNC angle of 100°. CIC-TDA results show a narrow S_1/S_0 gap around 0.2 eV at CNNC angles from 0° to 30° and a CoIn at a CNNC angle of 100°.

11-cis retinal protonated Schiff base (PSB11)

PSB11 is the chromophore of rhodopsin proteins. Rhodopsin is a light-sensitive protein that converts light into electrical signals that the brain interprets as vision. The biological activity of rhodopsins is triggered by the ultrafast light-induced $cis - trans$ isomerization of the corresponding retinal chromophores. In this process, the retinal chromophores transform the absorption of light into a physiological signal through conformational changes that initiate a complicated signaling cascade, resulting in electrical impulses sent to the brain and ultimately leading to visual perception.[89] The photoisomerization of the retinal chromophore has been intensively studied.[76,89–91] The reaction mechanism can be characterized by two modes (first stretching then torsion), and the corresponding photoisomerization path on the spectroscopic state S_1 essentially drives the system into a central double bond twisted S_1/S_0 CoIn.

Using a complete active space of 12 $\pi-$electrons in 12 $\pi-$orbitals with the 6-31G* basis set, unconstrained CASPT2/CASSCF minimum energy path (MEP) computations were performed in a previous study,[76] where the structure of the S_1/S_0 CoIn was found with a twisting angle of $-39°$ for the $\beta-$ionone ring and a rotation of $-80°$ about the $C_{11}-C_{12}$ double bond, as indicated in Fig.6(a).

To assess how well the CIC-TDA method describes the CoIn of PSB11, we computed the PESs of S_0 and S_1 along the estimated and extrapolated mass-weighted reaction coordinate ξ [bohr(amu)$^{1/2}$] based on that reported in Ref. 76. In particular, we used the coordinates of the $\beta-$ionone ring frozen ($PSB11_{frozen}$) structure provided in Ref. 76 and adjusted the bond lengths and torsion angles as indicated in Fig.6(a) according to the values in the Fig.2 of Ref. 76 for reaction coordinate $\xi \leq 21$. We further extrapolated the bond lengths and torsion angles up to ξ around 25. The results of the CASPT2, CIC-TDA/KS-SCF/KS-TDA methods are shown in Fig.6(b) and Fig.6(c). In Fig.6(b), the CASPT2 results predict a S_1/S_0 CoIn at $\xi \approx 20.5$, which is in line with the PESs obtained from CASPT2/CASSCF optimized reaction coordinate in Ref. 76.

In Fig.6(c), the overall profiles of PESs derived from KS-SCF/KS-TDA and CIC-TDA

results are consistent with that in Fig.6(b). The KS-SCF/KS-TDA results give a minimum-energy gap (MEG) around 0.44 eV at $\xi \approx 21.4$, whereas the CIC-TDA results increase this MEG to 1.07 eV without significantly changing the energy profiles far from this point.

In addition to comparing the KS-SCF/KS-TDA and CIC-TDA results discussed in Fig.6(c), we computed the PESs using the PBE33 functional (see Fig.S2 in Supporting Information). The MEG of S_0 and S_1 PESs derived from KS-SCF/KS-TDA becomes as small as 0.16 eV. However, the CIC-TDA method has the tendency to increase the MEG by decreasing and increasing the S_0 and S_1 PESs, respectively. Better descriptions of the PESs including MEG between S_0 and S_1 can be obtained with appropriate or improved xc functionals, for which the CIC-TDA method should correct the spurious crossing of KS-SCF/KS-TDA method at the S_1/S_0 CoIn point.

We note that the photoisomerization path on the spectroscopic state S_1 is essentially barrierless and drives the system into a central double bond twisted S_1/S_0 CoIn funnel according to the CASPT2/CASSCF results in Ref. 76. However, for the KS-SCF/KS-TDA and CIC-TDA results as shown in Fig.6(c), there is a barrier of around 0.7 eV characterized by the energy difference between ξ at 0 and 14. There is a charge-transfer process on S_1 upon photoexcitation,[76] where the positive charge migrates from the nitrogen-containing moiety towards the other half of the chromophore. Global hybrid functionals with a fixed fraction of HF exchange mixed with a local or semi-local xc functional are not optimal for describing both short-range and long-range interactions simultaneously. Range-separated functionals explicitly handle the distance dependence of interactions,[92–94] which makes them better suited for describing charge transfer processes. In order to demonstrate this, we calculated the PESs with the CAM-B3LYP[95,96] functional as shown in Fig.6(d). For the PES of the S_1 state, an extended energy plateau emerges from ξ at 0 up to 5 and the barrier of the energy difference between ξ at 0 and 14 is around 0.1 eV. Similar PES profiles and barriers of the S_1 state were also obtained with long-range corrected PBE (LC-PBE) and long-range PBE0 (LC-PBE0) functionals, respectively.[97–99] (see additional details in Fig.S3 and Fig.S4 in SI).

Further improvements may be possible with tuned range-separated functionals.[100–105]

Conclusions

We have shown that the CIC-TDA method, which includes the coupling between the ground state and the intersecting response excited state, can correct the artificial S_1/S_0 state crossings of the KS-SCF/KS-TDA method. We tested the CIC-TDA method from molecules ranging from small to relatively large, in particular, ammonia, ethylene, bithiophene, azobenzene, and the rhodopsin chromophore. The calculated PESs of S_1 and S_0, including the molecules for which PESs involving bond making and breaking processes, are comparable to those of multireference wave function methods. We performed TDDFT calculations with the PBE0 functional and calculated the CIC coupling element $A^{\mathrm{CIC}}_{0,ia}$ with HF exchange. Additionally, we assessed the efficacy of range-separated functionals in the rhodopsin chromophore system. In principle, the CIC-TDA method can be applied with any xc functional, thus further improving the accuracy as possible by using an appropriately selected functional or extensions. The CIC-TDA method is applicable to quite large molecules and can be considered as a promising alternative to semi-empirical and multireference wave function methods, making feasible the simulation of the photochemical dynamics of complex molecular systems. Future planned developments include nonadiabatic coupling vectors, which would allow the simulation of wave packet dynamics, and energy gradients, which would in turn allow the simulation of nonadiabatic molecular dynamics for larger molecular systems using curvature-driven trajectory surface hopping methods.[50,106]

Acknowledgement

This study was supported by the U.S. Department of Energy, Office of Science, Office of Basic Energy Sciences, Division of Chemical Sciences, Geosciences, and Biosciences under FWP 72684 (L.X., N.G. at the Pacific Northwest National Laboratory (PNNL)), DE-SC0022225

(V.M.F., S.M. at the University of California, Irvine and M.G. at the University of Bologna, Italy), and DE-SC0015997 (D.G.T. at the University of Minnesota). F.A. acknowledges financial support from the European Union – Next Generation EU – PNRR – M4C2, investimento 1.1 – "Fondo PRIN 2022" – "Understanding the pHotochemistry of sulfur substituted dnA bases by advanced ultrafast spectroscopy for phototherapeutic applications (HAPPY) ID P20224AWLB – CUP D53D23016720001". This work was performed in part at the Center for Integrated Nanotechnologies (CINT), a U.S. Department of Energy, Office of Science user facility at Los Alamos National Laboratory (LANL). The research benefited from computational resources provided by PNNL's Institutional Computing (PIC) Program, Environmental Molecular Sciences Laboratory (EMSL), a DOE Office of Science User Facility sponsored by the Office of Biological and Environmental Research and located at PNNL, and the National Energy Research Scientific Computing Center (NERSC), a U.S. Department of Energy Office of Science User Facility operated under Contract No. DE-AC02-05CH11231. PNNL is operated by Battelle Memorial Institute for the United States Department of Energy under DOE Contract No. DE-AC05-76RL1830.

Supporting Information Available

The following file is available free of charge.

- Filename: Supporting Information

The associated coordinates and geometric parameters of ammonia, ethylene, bithiophene, azobenzene, and PSB11 are provided. Additional figures demonstrating the PESs of ethylene and PSB11 using the PBE0 functional with the variation of the HF exchange fraction are included.

References

(1) Teller, E. The Crossing of Potential Surfaces. *J. Phys. Chem* **1937**, *41*, 109–116.

(2) Yarkony, D. R. Conical Intersections: Diabolical and Often Misunderstood. *Acc. Chem. Res.* **1998**, *31*, 511–518.

(3) Domcke, W.; Yarkony, D. R.; Köppel, H. *Conical intersections: electronic structure, dynamics and spectroscopy*; World Scientific, 2004; Vol. 15.

(4) Worth, G. A.; Cederbaum, L. S. Beyond Born-Oppenheimer: molecular dynamics through a conical intersection. *Annu. Rev. Phys. Chem.* **2004**, *55*, 127–158.

(5) Domcke, W.; Yarkony, D. R.; Köppel, H. *Conical intersections: theory, computation and experiment*; World Scientific, 2011; Vol. 17.

(6) Matsika, S.; Krause, P. Nonadiabatic Events and Conical Intersections. *Annu. Rev. Phys. Chem.* **2011**, *62*, 621–643.

(7) Mai, S.; González, L. Molecular photochemistry: Recent developments in theory. *Angew. Chem. Int. Ed.* **2020**, *59*, 16832–16846.

(8) Schuurman, M. S.; Stolow, A. Dynamics at conical intersections. *Annu. Rev. Phys. Chem.* **2018**, *69*, 427–450.

(9) Levine, B. G.; Esch, M. P.; Fales, B. S.; Hardwick, D. T.; Peng, W.-T.; Shu, Y. Conical intersections at the nanoscale: Molecular ideas for materials. *Annu. Rev. Phys. Chem.* **2019**, *70*, 21–43.

(10) Matsika, S. Electronic structure methods for the description of nonadiabatic effects and conical intersections. *Chem. Rev.* **2021**, *121*, 9407–9449.

(11) Cheng, Y.-C.; Fleming, G. R. Dynamics of Light Harvesting in Photosynthesis. *Ann. Rev. Phys. Chem.* **2009**, *60*, 241–262.

(12) Wenderich, K.; Mul, G. Methods, Mechanism, and Applications of Photodeposition in Photocatalysis: A Review. *Chem. Rev.* **2016**, *116*, 14587–14619.

(13) Schoenlein, R. W.; Peteanu, L. A.; Mathies, R. A.; Shank, C. V. The First Step in Vision: Femtosecond Isomerization of Rhodopsin. *Science* **1991**, *254*, 412–415.

(14) Polli, D.; Altoè, P.; Weingart, O.; Spillane, K. M.; Manzoni, C.; Brida, D.; Tomasello, G.; Orlandi, G.; Kukura, P.; Mathies, R. A.; Garavelli, M.; Cerullo, G. Conical intersection dynamics of the primary photoisomerization event in vision. *Nature* **2010**, *467*, 440–443.

(15) Sinha, R. P.; Höder, D.-P. UV-induced DNA damage and repair: a review. *Photochem. Photobiol. Sci.* **2002**, *1*, 225–236.

(16) Schultz, T.; Samoylova, E.; Radloff, W.; Hertel, I. V.; Sobolewski, A. L.; Domcke, W. Efficient Deactivation of a Model Base Pair via Excited-State Hydrogen Transfer. *Science* **2004**, *306*, 1765–1768.

(17) Middleton, C. T.; de La Harpe, K.; Su, C.; Law, Y. K.; Crespo-Hernández, C. E.; Kohler, B. DNA excited-state dynamics: from single bases to the double helix. *Annu. Rev. Phys. Chem.* **2009**, *60*, 217–239.

(18) Gozem, S.; Melaccio, F.; Valentini, A.; Filatov, M.; Huix-Rotllant, M.; Ferré, N.; Frutos, L. M.; Angeli, C.; Krylov, A. I.; Granovsky, A. A.; Lindh, R.; Olivucci, M. Shape of Multireference, Equation−of−Motion Coupled−Cluster, and Density Functional Theory Potential Energy Surfaces at a Conical Intersection. *J. Chem. Theory Comput.* **2014**, *10*, 3074–3084.

(19) Fdez. Galván, I. and Delcey, M. G. and Pedersen, T. B. and Aquilante, F. and Lindh, R. Analytical State−Average Complete−Active−Space Self−Consistent Field Nonadiabatic Coupling Vectors: Implementation with Density−Fitted Two−Electron Inte-

grals and Application to Conical Intersections. *J. Chem. Theory Comput.* **2016**, *12*, 3636–3653.

(20) Andersson, K.; Malmqvist, P. A.; Roos, B.; Sadlej, A. J.; Wolinski, K. Second-order perturbation theory with a CASSCF reference function. *J. Phys. Chem.* **1990**, *94*, 5483–5488.

(21) Helgaker, T.; Jørgensen, P.; Olsen, J. *Molecular Electronic-Structure Theory*; Wiley, Chichester, 2000.

(22) Shiozaki, T.; Werner, H.-J. Explicitly correlated multireference configuration interaction with multiple reference functions: Avoided crossings and conical intersections. *J. Chem. Phys.* **2011**, *134*, 184104.

(23) Werner, H.-J.; Knowles, P. J. An efficient internally contracted multiconfiguration-reference configuration interaction method. *J. Chem. Phys.* **1988**, *89*, 5803–5814.

(24) Kohn, W.; Sham, L. J. Self-consistent equations including exchange and correlation effects. *Physical review* **1965**, *140*, A1133.

(25) Parr, R. G.; Weitao, Y. *Density-Functional Theory of Atoms and Molecules*; Oxford University Press, USA, 1994.

(26) Casida, M. E. In *Recent Advances In Density Functional Methods: (Part I)*; Chong, D. P., Ed.; World Scientific, 1995; pp 155–192.

(27) Ullrich, C. A. Time-Dependent Density-Functional Theory: Concepts and Applications. **2011**,

(28) Foresman, J. B.; Head-Gordon, M.; Pople, J. A.; Frisch, M. J. Toward a systematic molecular orbital theory for excited states. *J. Phys. Chem.* **1992**, *96*, 135–149.

(29) Szabo, A.; Ostlund, N. S. *Modern Quantum Chemistry: Introduction to Advanced Electronic Structure Theory*; McGraw-Hill, Inc.: New York, 1989.

(30) Levine, B. G.; Ko, C.; Quenneville, J.; Martínez, T. J. Conical intersections and double excitations in time−dependent density functional theory. *Mol. Physical.* **2006**, *104*, 1039–1051.

(31) Mayer, I. *Simple theorems, proofs, and derivations in quantum chemistry*; Springer Science & Business Media, 2013.

(32) Plasser, F.; Crespo-Otero, R.; Pederzoli, M.; Pittner, J.; Lischka, H.; Barbatti, M. Surface Hopping Dynamics with Correlated Single−Reference Methods: 9H−Adenine as a Case Study. *J. Chem. Theory Comput.* **2014**, *10*, 1395–1405.

(33) Lefrancois, D.; Tuna, D.; Martínez, T. J.; Dreuw, A. The Spin−Flip Variant of the Algebraic−Diagrammatic Construction Yields the Correct Topology of S_1/S_0 Conical Intersections. *J. Chem. Theory Comput.* **2017**, *13*, 4436–4441.

(34) Köhn, A. and Tajti, A. Can coupled−cluster theory treat conical intersections? *J. Chem. Phys.* **2007**, *127*, 044105.

(35) Kjønstad, Eirik F. and Myhre, Rolf H. and Martínez, Todd J. and Koch, Henrik Crossing conditions in coupled cluster theory. *J. Chem. Phys.* **2017**, *147*, 164105.

(36) Rossi, F.; Kjønstad, E. F.; Angelico, S.; Koch, H. Generalized coupled cluster theory for ground and excited state intersections. *arXiv preprint arXiv:2411.08751* **2024**,

(37) Grimme, S.; Waletzke, M. A combination of Kohn–Sham density functional theory and multi-reference configuration interaction methods. *J. Chem. Phys.* **1999**, *111*, 5645–5655.

(38) Gräfenstein, J.; Cremer, D. Development of a CAS-DFT method covering non-dynamical and dynamical electron correlation in a balanced way. *Mol. Phys.* **2005**, *103*, 279–308.

(39) Shao, Y. and Head-Gordon, M. and Krylov, A. I. The spin–flip approach within time-dependent density functional theory: Theory and applications to diradicals. *J. Chem. Phys.* **2003**, *118*, 4807–4818.

(40) Casanova, D.; Krylov, A. I. Spin-flip methods in quantum chemistry. *Phys. Chem. Chem. Phys.* **2020**, *22*, 4326–4342.

(41) Minezawa, N.; Gordon, M. S. Optimizing Conical Intersections by Spin−Flip Density Functional Theory: Application to Ethylene. *J. Phys. Chem. A* **2009**, *113*, 12749–12753.

(42) Minezawa, N.; Gordon, M. S. Photoisomerization of Stilbene: A Spin−Flip Density Functional Theory Approach. *J. Phys. Chem. A* **2011**, *115*, 7901–7911.

(43) Zhang, X.; Herbert, J. M. Excited-State Deactivation Pathways in Uracil versus Hydrated Uracil: Solvatochromatic Shift in the $1n\pi^*$ State is the Key. *J. Phys. Chem. B* **2014**, *118*, 7806–7817.

(44) Park, W.; Komarov, K.; Lee, S.; Choi, C. H. Mixed-Reference Spin-Flip Time-Dependent Density Functional Theory: Multireference Advantages with the Practicality of Linear Response Theory. *J. Phys. Chem. Lett.* **2023**, *14*, 8896–8908.

(45) Gagliardi, L.; Truhlar, D. G.; Li M., G.; Carlson, R. K.; Hoyer, C. E.; Bao, J. L. Multiconfiguration Pair-Density Functional Theory: A New Way To Treat Strongly Correlated Systems. *Acc. Chem. Res.* **2017**, *50*, 66–73.

(46) Sand, A. M.; Hoyer, C. E.; Truhlar, D. G.; Gagliardi, L. State-interaction pair-density functional theory. *J. Chem. Phys.* **2018**, *149*, 024106.

(47) Bao, J. J.; Zhou, C.; Truhlar, D. G. Compressed-State Multistate Pair-Density Functional Theory. *J. Chem. Theory Comput.* **2020**, *16*, 7444–7452.

(48) Calio, P. B.; Hermes, M. R.; Bao, J. J.; Galván, I. F.; Lindh, R.; Truhlar, D. G.; Gagliardi, L. Minimum−Energy Conical Intersections by Compressed Multistate Pair−Density Functional Theory. *J. Phys. Chem. A*. **2024**, *128*, 1698–1706.

(49) Hennefarth, M. R.; Hermes, M. R.; Truhlar, D. G.; Gagliardi, L. Linearized Pair−Density Functional Theory. *J. Chem. Theory Comput.* **2023**, *19*, 3172–3183.

(50) Hennefarth, M. R.; Truhlar, D. G.; Gagliardi, L. Semiclassical Nonadiabatic Molecular Dynamics Using Linearized Pair−Density Functional Theory. *J. Chem. Theory Comput.* **2024**, *20*, 8741–8748.

(51) Maitra, N. T.; Zhang, F.; Cave, R. J.; Burke, K. Double excitations within time−dependent density functional theory linear response. *J. Chem. Phys.* **2004**, *120*, 5932–5937.

(52) Cave, R. J.; Zhang, F.; Maitra, N. T.; Burke, K. A dressed TDDFT treatment of the 2^1A_g states of butadiene and hexatriene. *Chem. Phys. Lett.* **2004**, *389*, 39–42.

(53) Huix-Rotllant, M.; Ipatov, A.; Rubio, A.; Casida, M. E. Assessment of dressed time-dependent density-functional theory for the low-lying valence states of 28 organic chromophores. *Chem. Phys.* **2011**, *391*, 120–129.

(54) Teh, H.-H.; Subotnik, J. E. The Simplest Possible Approach for Simulating S_0-S_1 Conical Intersections with DFT/TDDFT: Adding One Doubly Excited Configuration. *J. Phys. Chem. Lett.* **2019**, *10*, 3426–3432.

(55) Athavale, V.; Teh, H.-H.; Subotnik, J. E. On the inclusion of one double within CIS and TDDFT. *J. Chem. Phys.* **2021**, *155*, 154105.

(56) Li, S. L.; Marenich, A. V.; Xu, X.; Truhlar, D. G. Configuration Interaction-Corrected Tamm–Dancoff Approximation: A Time-Dependent Density Functional Method with

the Correct Dimensionality of Conical Intersections. *J. Phys. Chem. Lett.* **2014**, *5*, 322–328.

(57) Shu, Y.; Parker, K. A.; Truhlar, D. G. Dual−Functional Tamm−Dancoff Approximation: A Convenient Density Functional Method that Correctly Describes S_1/S_0 Conical Intersections. *J. Phys. Chem. Lett.* **2017**, *8*, 2107–2112.

(58) Onida, G.; Reining, L.; Rubio, A. Electronic excitations: density-functional versus many-body Green's-function approaches. *Rev. Mod. Phys.* **2002**, *74*, 601–659.

(59) Dreuw, A.; Head-Gordon, M. Single-Reference ab Initio Methods for the Calculation of Excited States of Large Molecules. *Chem. Rev.* **2005**, *105*, 4009–4037.

(60) Bauernschmitt, R.; Ahlrichs, R. Treatment of electronic excitations within the adiabatic approximation of time dependent density functional theory. *Chem. Phys. Lett.* **1996**, *256*, 454–464.

(61) Hirata, S.; Head-Gordon, M. Time-dependent density functional theory within the Tamm–Dancoff approximation. *Chem. Phys. Lett.* **1999**, *314*, 291–299.

(62) Casida, M.; Huix-Rotllant, M. Progress in Time−Dependent Density−Functional Theory. *Annu. Rev. Phys. Chem.* **2012**, *63*, 287–323.

(63) Zhao, X.; Merritt, I.; Lei, R.; Shu, Y.; Jacquemin, D.; Zhang, L.; Xu, X.; Vacher, M.; Truhlar, D. G. Nonadiabatic coupling in trajectory surface hopping: accurate time derivative couplings by the curvature-driven approximation. *J. Chem. Theory Comput.* **2023**, *19*, 6577–6588.

(64) Papineau, T. V.; Jacquemin, D.; Vacher, M. Which Electronic Structure Method to Choose in Trajectory Surface Hopping Dynamics Simulations? Azomethane as a Case Study. *J. Phys. Chem. Lett.* **2024**, *15*, 636–643.

(65) Davidson, E. R. The iterative calculation of a few of the lowest eigenvalues and corresponding eigenvectors of large real-symmetric matrices. *J. Computational Physics* **1975**, *17*, 87–94.

(66) Hehre, W. J.; Ditchfield, R.; Pople, J. A. Self—consistent molecular orbital methods. XII. Further extensions of Gaussian—type basis sets for use in molecular orbital studies of organic molecules. *J. Chem. Phys.* **1972**, *56*, 2257–2261.

(67) Hariharan, P. C.; Pople, J. A. The influence of polarization functions on molecular orbital hydrogenation energies. *Theor. Chim. Acta* **1973**, *28*, 213–222.

(68) Clark, T.; Chandrasekhar, J.; Spitznagel, G. W.; von Ragué Schleyer, P. Efficient diffuse function-augmented basis sets for anion calculations. III. The 3−21+G basis set for first-row elements, Li−F. *J. Comput. Chem.* **1983**, *4*.

(69) Valiev, M.; Bylaska, E.; Govind, N.; Kowalski, K.; Straatsma, T.; Van Dam, H.; Wang, D.; Nieplocha, J.; De Jong, W.; Apra, E.; others NWChem: A comprehensive and scalable open-source solution for large scale molecular simulations. *Computer Physics Communications* **2010**, *181*, 1477–1489.

(70) Aprà, E. et al. NWChem: Past, present, and future. *J. Chem. Phys.* **2020**, *152*, 184102.

(71) Adamo, C.; Barone, V. Toward reliable density functional methods without adjustable parameters: The PBE0 model. *J. Chem. Phys.* **1999**, *110*, 6158–6170.

(72) Cortona, P. Note: Theoretical mixing coefficients for hybrid functionals. *J. Chem. Phys.* **2012**, *136*.

(73) Guido, C. A.; Brémond, E.; Adamo, C.; Cortona, P. Communication: One third: A new recipe for the PBE0 paradigm. *J. Chem. Phys.* **2013**, *138*.

(74) Werner, H. J.; Knowles, P. J.; Knizia, G.; Manby, F. R.; Schütz, M. Molpro: A general-purpose quantum chemistry program package. *Wiley Rev: Comp. Mol. Sci.* **2012**, *2*, 242–253.

(75) Li Manni, G. et al. The OpenMolcas Web: A Community-Driven Approach to Advancing Computational Chemistry. *J. Chem. Theory Comput.* **2023**, *19*, 6933–6991.

(76) Cembran, A. and González-Luque, R. and Serrano-Andrés, L. and Merchán, M. and Garavelli, M. About the intrinsic photochemical properties of the 11-cis retinal chromophore: computational clues for a trap state and a lever effect in Rhodopsin catalysis. *Theor. Chem. Acc.* **2007**, *118*, 173–183.

(77) Nangia, S.; Truhlar, D. G.; McGuire, M. J.; Piecuch, P. Can a single-reference approach provide a balanced description of ground and excited states? A comparison of the completely renormalized equation-of-motion coupled-cluster method with multireference quasidegenerate perturbation theory near a conical intersection and along a photodissociation coordinate in ammonia. *J. Phys. Chem. A.* **2005**, *109*, 11643–11646.

(78) Nangia, S.; Truhlar, D. G. Direct calculation of coupled diabatic potential-energy surfaces for ammonia and mapping of a four-dimensional conical intersection seam. *J. Chem. Phys.* **2006**, *124*.

(79) Li, Z. H.; Valero, R.; Truhlar, D. G. Improved direct diabatization and coupled potential energy surfaces for the photodissociation of ammonia. *Theor. Chem. Acc.* **2007**, *118*, 9–24.

(80) Ben-Nun, M.; Martınez, T. J. Ab initio molecular dynamics study of cis–trans photoisomerization in ethylene. *Chem. Phys. Lett.* **1998**, *298*, 57–65.

(81) Ben-Nun, M.; Martınez, T. J. Photodynamics of ethylene: ab initio studies of conical intersections. *Chem. Phys.* **2000**, *259*, 237–248.

(82) Nikiforov, A.; Gamez, J. A.; Thiel, W.; Huix-Rotllant, M.; Filatov, M. Assessment of approximate computational methods for conical intersections and branching plane vectors in organic molecules. *J. Chem. Phys.* **2014**, *141*.

(83) Yu, J. K.; Bannwarth, C.; Hohenstein, E. G.; Martínez, T. J. Ab initio nonadiabatic molecular dynamics with hole–hole Tamm–Dancoff approximated density functional theory. *J. Chem. Theory Comput.* **2020**, *16*, 5499–5511.

(84) Kölle, P.; Schnappinger, T.; de Vivie-Riedle, R. Deactivation pathways of thiophene and oligothiophenes: internal conversion versus intersystem crossing. *Phys. Chem. Chem. Phys.* **2016**, *18*, 7903–7915.

(85) Barbarella, G.; Melucci, M.; Sotgiu, G. The Versatile Thiophene: An Overview of Recent Research on Thiophene−Based Materials. *Adv. Mater.* **2005**, *17*, 1581–1593.

(86) Grimsdale, A. C.; Leok Chan, K.; Martin, R. E.; Jokisz, P. G.; Holmes, A. B. Synthesis of Light−Emitting Conjugated Polymers for Applications in Electroluminescent Devices. *Chem. Rev.* **2009**, *109*, 897–1091.

(87) Günes, S.; Neugebauer, H.; Sariciftci, N. S. Conjugated Polymer−Based Organic Solar Cells. *Chem. Rev.* **2007**, *107*, 1324–1338.

(88) Aleotti, F.; Soprani, L.; Nenov, A.; Berardi, R.; Arcioni, A.; Zannoni, C.; Garavelli, M. Multidimensional Potential Energy Surfaces Resolved at the RASPT2 Level for Accurate Photoinduced Isomerization Dynamics of Azobenzene. *J. Chem. Theory Comput.* **2019**, *15*, 6813–6823.

(89) Gruhl, T. et al. Ultrafast structural changes direct the first molecular events of vision. *Nature* **2023**, *615*, 939–944.

(90) Tomasello, G. and Olaso-González, G. and Altoè, P. and Stenta, M. and Serrano-Andrés, L. and Merchán, M. and Orlandi, G. and Bottoni, A. and Garavelli, M.

Electrostatic Control of the Photoisomerization Efficiency and Optical Properties in Visual Pigments: On the Role of Counterion Quenching. *J. Am. Chem. Soc.* **2009**, *131*, 5172–5186.

(91) Polli, D. and Altoè, P. and Weingart, O. and Spillane, K. M. and Manzoni, C. and Brida, D. and Tomasello, G. and Orlandi, G. and Kukura, P. and Mathies, R. A. and Garavelli, M. and Cerullo, G. Conical intersection dynamics of the primary photoisomerization event in vision. *Nature* **2010**, *467*, 440–443.

(92) Iikura, H.; Tsuneda, T.; Yanai, T.; Hirao, K. A long-range correction scheme for generalized-gradient-approximation exchange functionals. *J. Chem. Phys.* **2001**, *115*, 3540–3544.

(93) Toulouse, J.; Colonna, F.; Savin, A. Long-range–short-range separation of the electron-electron interaction in density-functional theory. *Phys. Rev. A* **2004**, *70*, 062505.

(94) Kronik, L.; Kümmel, S. Piecewise linearity, freedom from self-interaction, and a Coulomb asymptotic potential: three related yet inequivalent properties of the exact density functional. *Phys. Chem. Chem. Phys.* **2020**, *22*, 16467–16481.

(95) Yanai, T.; Tew, D. P.; Handy, N. C. A new hybrid exchange–correlation functional using the Coulomb-attenuating method (CAM-B3LYP). *Chem. Phys. Lett.* **2004**, *393*, 51–57.

(96) Peach, M. J. G.; Cohen, A. J.; Tozer, D. J. Influence of Coulomb-attenuation on exchange–correlation functional quality. *Phys. Chem. Chem. Phys.* **2006**, *8*, 4543–4549.

(97) Song, J.-W.; Hirosawa, T.; Tsuneda, T.; Hirao, K. Long−range corrected density functional calculations of chemical reactions: Redetermination of parameter. *J. Chem. Phys.* **2006**, *126*, 154105.

(98) Rohrdanz, M. A.; Herbert, J. M. Simultaneous benchmarking of ground− and excited−state properties with long−range−corrected density functional theory. *J. Chem. Phys.* **2008**, *129*, 034107.

(99) Baer, R.; Livshits, E.; Salzner, U. Tuned Range−Separated Hybrids in Density Functional Theory. *Annu. Rev. Phys. Chem.* **2010**, *61*, 85–109.

(100) Stein, T.; Kronik, L.; Baer, R. Reliable prediction of charge transfer excitations in molecular complexes using time-dependent density functional theory. *J. Am. Chem. Soc.* **2009**, *131*, 2818–2820.

(101) Baer, R.; Livshits, E.; Salzner, U. Tuned range-separated hybrids in density functional theory. *Annu. Rev. Phys. Chem.* **2010**, *61*, 85–109.

(102) Refaely-Abramson, S.; Sharifzadeh, S.; Govind, N.; Autschbach, J.; Neaton, J. B.; Baer, R.; Kronik, L. Quasiparticle Spectra from a Nonempirical Optimally Tuned Range-Separated Hybrid Density Functional. *Phys. Rev. Lett.* **2012**, *109*, 226405.

(103) Lopata, K.; Govind, N. Near and Above Ionization Electronic Excitations with Non-Hermitian Real-Time Time-Dependent Density Functional Theory. *J. Chem. Theory Comput.* **2013**, *9*, 4939–4946.

(104) Autschbach, J.; Srebro, M. Delocalization error and "functional tuning" in Kohn–Sham calculations of molecular properties. *Acc. Chem. Res.* **2014**, *47*, 2592–2602.

(105) Prokopiou, G.; Hartstein, M.; Govind, N.; Kronik, L. Optimal tuning perspective of range-separated double hybrid functionals. *J. Chem. Theory Comput.* **2022**, *18*, 2331–2340.

(106) Shu, Y.; Zhang, L.; Chen, X.; Sun, S.; Huang, Y.; Truhlar, D. G. Nonadiabatic dynamics algorithms with only potential energies and gradients: Curvature-driven coherent

switching with decay of mixing and curvature-driven trajectory surface hopping. *J. Chem. Theory Comput.* **2022**, *18*, 1320–1328.

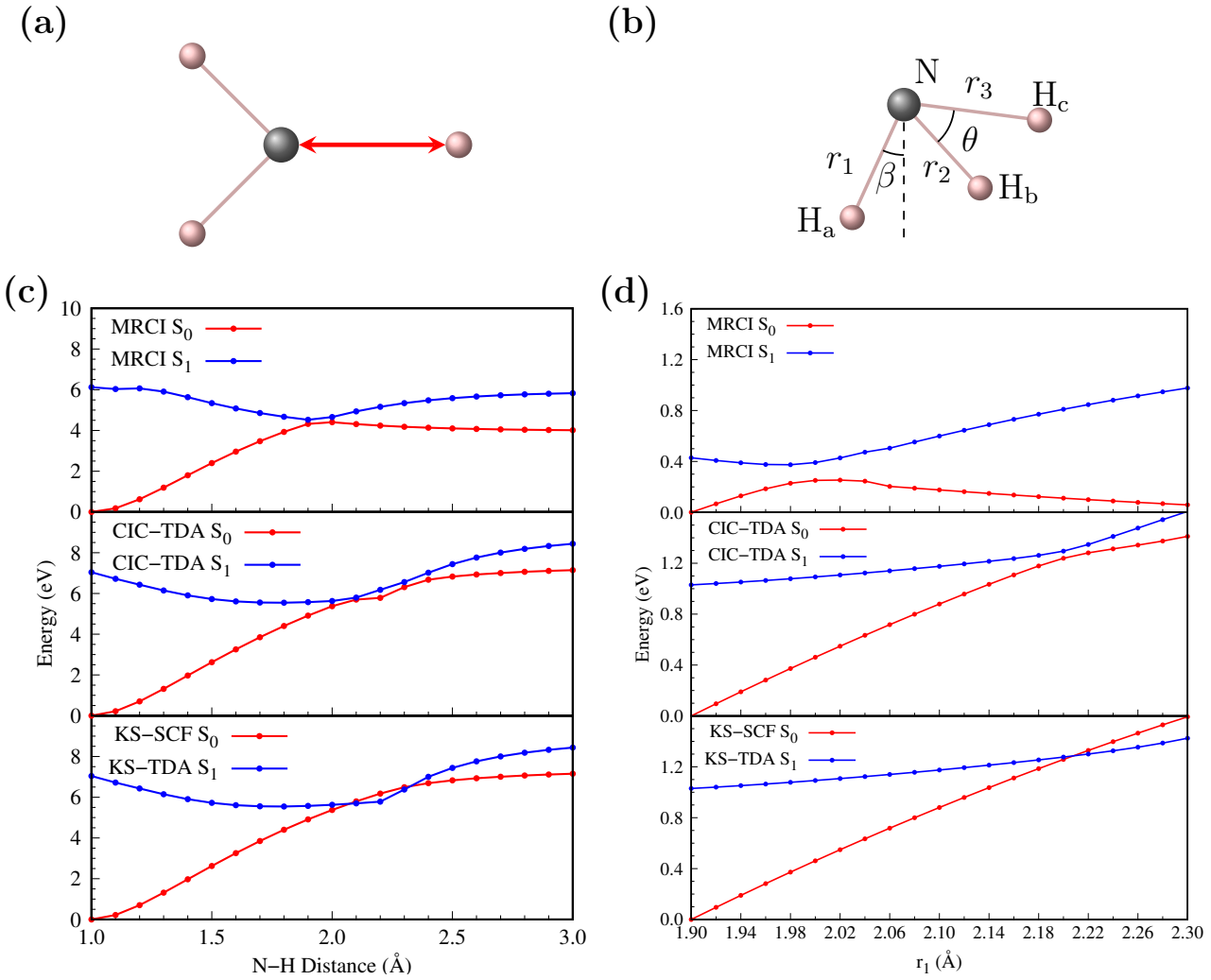

Figure 1: (a) Geometry of planar NH_3 with the distance of N−H dissociation. (b) Geometry of NH_3 with N−H bond stretching r_1 at $\beta = 89°$. Nitrogen and hydrogen atoms are represented by gray and pink colors, respectively. (c-d) PESs of NH_3 near S_1/S_0 conical intersection along the N−H dissociation distance and N−H bond stretching r_1 as calculated by MRCI, CIC-TDA, and KS-SCF/KS-TDA methods.

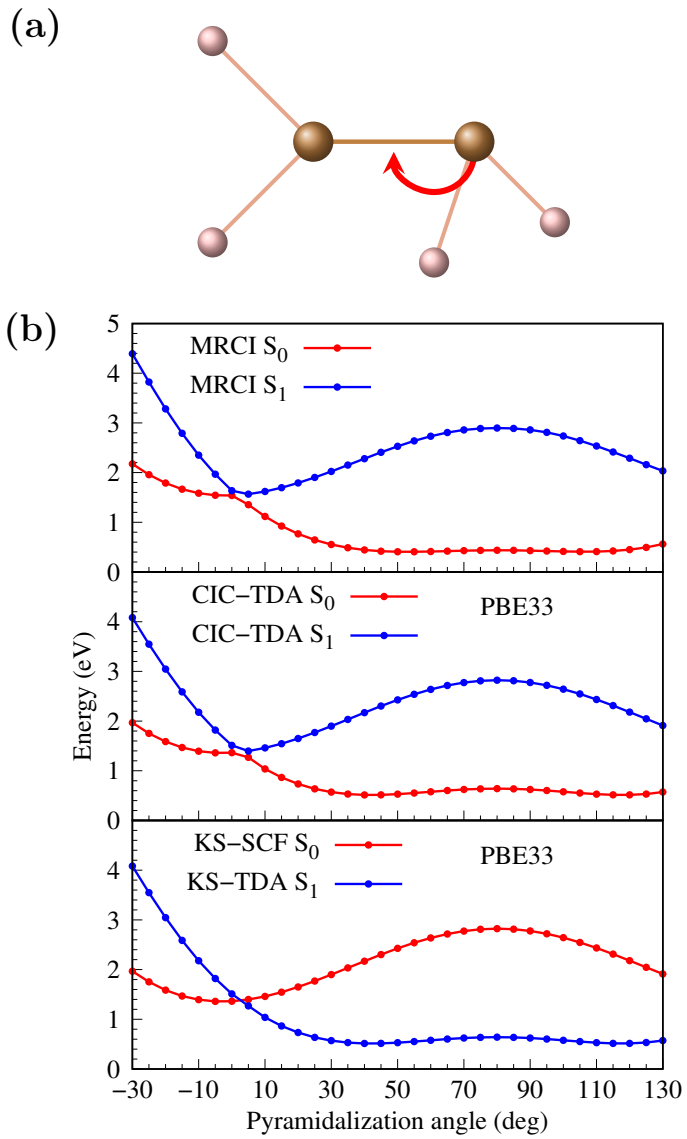

Figure 2: (a) Geometry of pyramidalization with carbon and hydrogen atoms represented by brown and pink colors, respectively. (b) PESs of C_2H_4 near S_1/S_0 conical intersection along the pyramidalization angle as calculated by MRCI, CIC-TDA, and KS-SCF/KS-TDA methods. For the CIC-TDA and KS-SCF/KS-TDA calculations, the PBE33 functional ($c_{\mathrm{HF}} = 0.33$) was used.

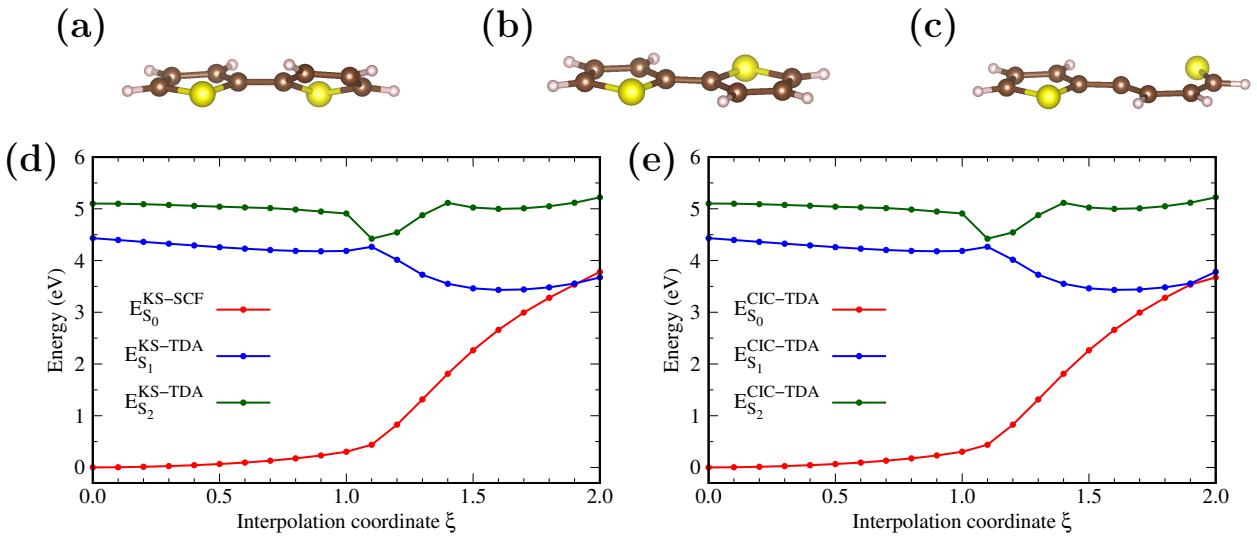

Figure 3: (a-c) Optimized geometries of bithiophene molecule in Ref. 84 including: (a) the optimized ground state geometry at the B3LYP/6-311** level S_0-min, two S_1 minimum structures at the CASSCF/6-31* level: (b) S_1-min-a, and (c) S_1-min-b. Carbon, sulfur, and hydrogen atoms are represented by brown, yellow, and pink colors, respectively. (d-e) Potential energy surfaces for the S_0, S_1, and S_2 states of the bithiophene molecule along the linear interpolation coordinate ξ calculated using PBE0/KS-SCF/KS-TDA (left) and PBE0/CIC-TDA (right). The interpolation coordinate $\xi = 0$ corresponds to the geometry of S_0-min, $\xi = 1$ corresponds to the geometry of S_1- min-a and $\xi = 2$ corresponds to the geometry of S_1-min-b. For KS-SCF/KS-TDA, there is a conical intersection with unphysical crossing at $\xi = 1.9$. For CIC-TDA, this conical intersection is corrected to an avoided crossing.

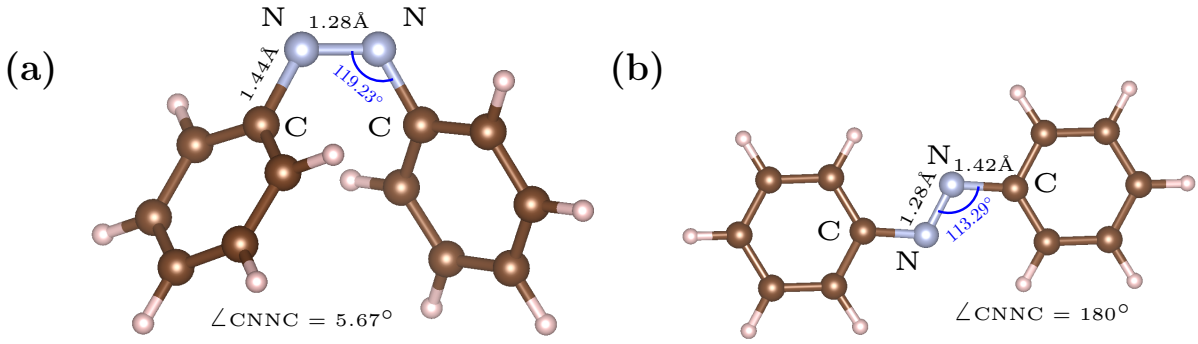

Figure 4: (a-b) The optimized geometries of gas phase azobenzene in Ref. 88: (a) *cis*-azobenzene, and (b) *trans*-azobenzene. The CNNC torsion and NNC/CNN symmetric angles are indicated. Carbon, nitrogen, and hydrogen atoms are represented by brown, gray, and pink colors, respectively.

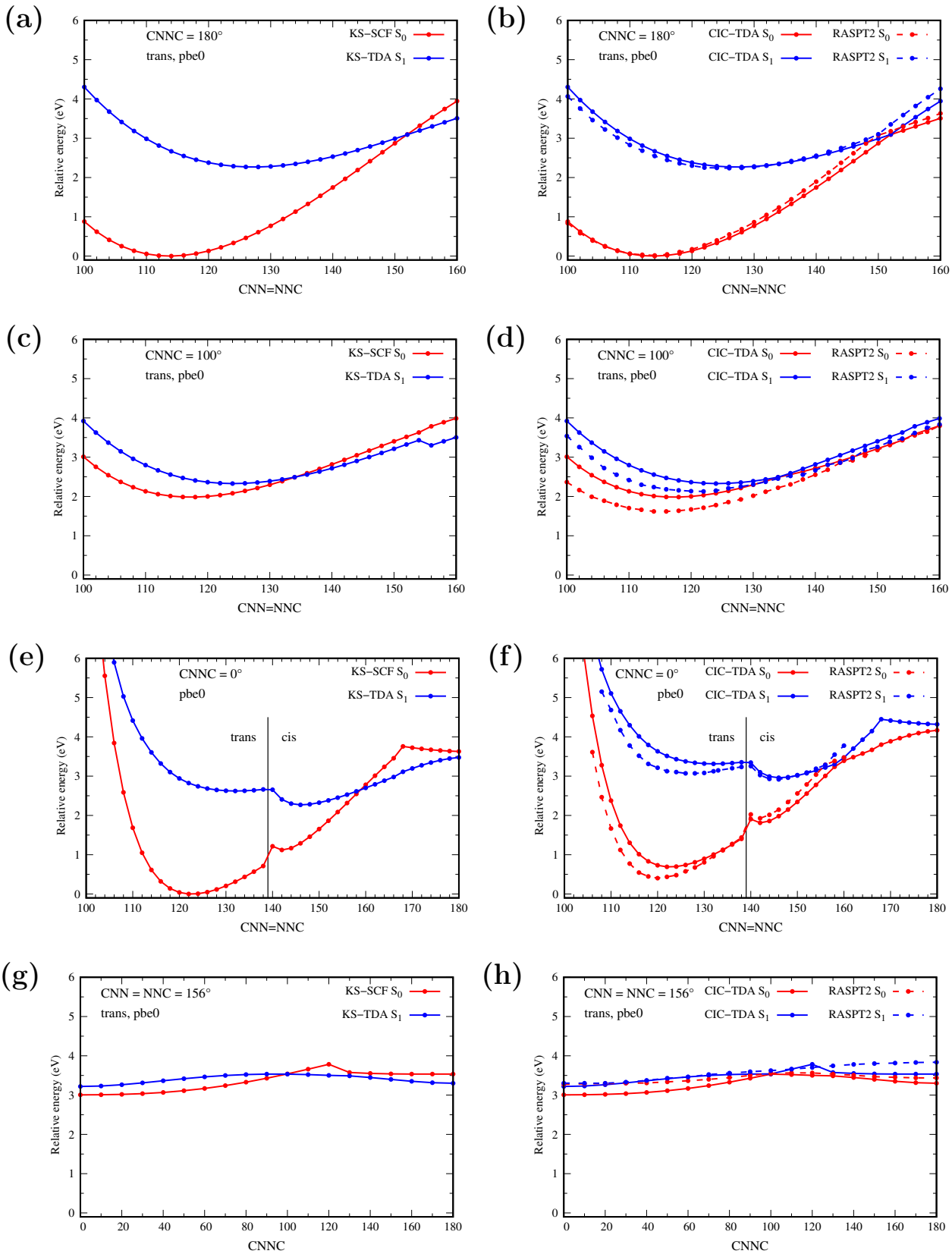

Figure 5: (a-h) Azobenzene PESs in the space of CNNC torsion and symmetric CNN bending angles as calculated by KS-SCF/KS-TDA, CIC-TDA, and RASPT2 methods. The dashed lines corresponding to the RASPT2 results were digitalized from Ref. 88. The regions calculated from the *trans*- and *cis*-derived coordinates are separated by vertical black lines in (e-f).

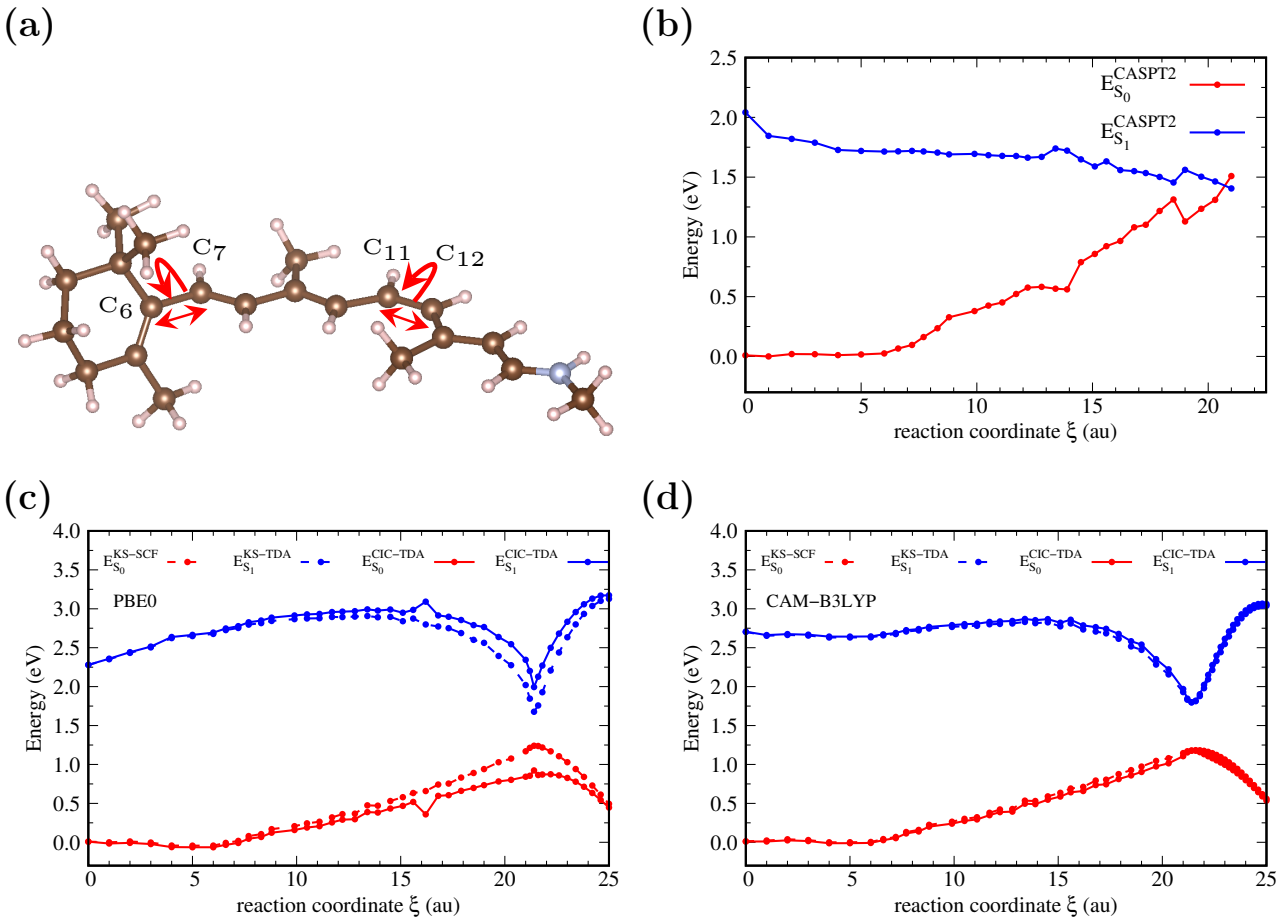

Figure 6: (a) Geometry of PSB11 with carbon, hydrogen, and nitrogen atoms represented by brown, pink, and gray colors, respectively. The red arrows indicate the stretching and torsion of C_6-C_7 and $C_{11}-C_{12}$ bonds along the CASSCF/6-31G* optimized reaction coordinate as reported in Ref. 76, *i.e.,* the twisting of the $\beta-$ionone ring on C_6-C_7 single bond and rotation about the $C_{11}-C_{12}$ double bond. (b) CASPT2-calculated PESs of PSB11 near S_1/S_0 conical intersection along the reaction coordinate ξ estimated based on that reported in Ref. 76. We used the coordinates of $\beta-$ionone ring frozen ($PSB11_{frozen}$) structure provided in Ref. 76 and adjusted the bond lengths and torsion angles as indicated in (a) according to the values in the Fig.2 of Ref. 76. (c,d) The PESs calculated with KS-SCF/KS-TDA and CIC-TDA methods along the estimated and extrapolated reaction coordinate ξ using PBE0 and CAM-B3LYP functionals, respectively. The geometries of the reaction coordinates $\xi \leq 21$ are the same as these in (b). The geometries of reaction coordinates $\xi > 21$ were extrapolated.